Heliyon 10 (2024) e40621

Contents lists available at ScienceDirect

Heliyon

journal homepage: www.cell.com/heliyon

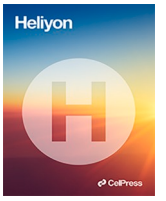

Research article

Mitochondrial dysfunction of Astrocyte induces cell activation under high salt condition

Yuemin Qiu [a,b,1], Gengxin Lu [a,1], Shifeng Zhang [a], Li Minping [a], Xu Xue [a], Wu Junyu [a], Zhihui Zheng [a], Weiwei Qi [a], Junjie Guo [a], Dongxiao Zhou [a], Haiwei Huang [a,**], Zhezhi Deng [a,*]

[a] *Department of Neurology, The First Affiliated Hospital, Sun Yat-sen University, Guangdong Provincial Key Laboratory of Diagnosis and Treatment of Major Neurological Diseases, National Key Clinical Department and Key Discipline of Neurology, No.58 Zhongshan Road 2, Guangzhou, 510080, China*

[b] *Department of Neurology, Shenzhen Bao'an District Songgang People's Hospital, No.2 Shajiang Road, Shenzhen, 518100, China*

ARTICLE INFO

Keywords:
Astrocyte
Mitochondrial dysfunction
High salt
TSPO ligand

ABSTRACT

Excess dietary sodium can accumulate in brain and adversely affect human health. We have confirmed in previous studies that high salt can induce activation of astrocyte manifested by the secretion of various inflammatory factors. In order to further explore the effect of high salt on the internal cell metabolism of astrocytes, RNA sequencing was performed on astrocytes under high salt environment, which indicated the oxidative phosphorylation and glycolysis pathways of astrocytes were downregulated. Next, we found that high salt concentrations elicited astrocyte mitochondrial morphology change, as evidenced by swelling from a short rod to a round shape through a High Intelligent and Sensitive Structured Illumination Microscope (HIS-SIM). Furthermore, we found that high salt concentrations reduced astrocyte mitochondrial oxygen consumption and membrane potential. Treatment with 18-kDa translocator protein (TSPO) ligands FGIN-1-27 improved mitochondrial networks and reversed astrocyte activation under high-salt circumstances. Our study shows that high salt can directly disrupt astrocytic mitochondrial homeostasis and function. Targeting translocator protein signaling may have therapeutic potential against high-salt neurotoxicity.

1. Introduction

In contemporary dietary practices, the consumption of salt, scientifically referred to as sodium chloride (NaCl), greatly surpasses the recommended thresholds [1,2]. The consumption of a diet high in salt, commonly referred to as a high-salt diet (HSD), has been widely acknowledged as a potential contributing factor to the development of numerous vascular diseases, including acute ischemic stroke and coronary heart disease. The primary recommendations for reducing dietary sodium (Na+) intake are primarily derived from scientific studies that have demonstrated a positive correlation between Na + consumption and systolic blood pressure (BP) [3,4]. However, recent studies have indicated that the accumulation of high levels of sodium ions (Na+) in the interstitium of the human

* Corresponding author. Sun Yat-sen University Guangzhou, China.
** Corresponding author. Sun Yat-sen University Guangzhou, China.
E-mail addresses: huanghw@mail.sysu.edu.cn (H. Huang), dengzhzh5@mail.sysu.edu.cn (Z. Deng).
[1] These authors contributed equally to this work.

https://doi.org/10.1016/j.heliyon.2024.e40621
Received 3 November 2023; Received in revised form 20 November 2024; Accepted 20 November 2024
Available online 21 November 2024

body can have detrimental effects on different target organs. These effects occur through mechanisms that are not related to blood pressure regulation, but rather involve the modulation of immune responses and the promotion of inflammation [5–7].

Due to the meticulous renal control over plasma electrolytes, the prolonged ingestion of an excessive amount of sodium may not result in an elevation of plasma sodium levels. However, it can lead to the accumulation of sodium in the interstitial spaces of the human body, irrespective of the kidney's influence. Significantly, the sodium concentration within the interstitium of the human body is approximately 40 mM (mM) greater than the sodium concentration within the plasma [8]. The central nervous system (CNS) is a primary site of susceptibility to the detrimental effects caused by excessive salt exposure. Astrocytes, being the predominant interstitial cells within the central nervous system, exhibit a remarkable capacity to promptly adapt to alterations within the microenvironment [9,10]. As one of the most abundant and widely distributed glial cells in the central nervous system, astrocytes exhibit a multitude of essential roles. These encompass the intricate regulation of synapse quantities, synaptic transmission, cerebral blood flow within the central nervous system, permeability of the blood-brain barrier, and the maintenance of energy balance in the central nervous system [11–13].

Our previous studies have shown that high salt can induce astrocyte activation and secrete a variety of inflammatory factors, suggesting a direct impact of high salt on their functional state [14]. They exhibit the highest susceptibility to direct impact from elevated salt levels. This activation process involves changes in astrocytic morphology and physiology that can influence microvascular permeability and the integrity of the blood-brain barrier [15]. However, the effect of high salt on the internal structure of astrocytes is still unknown. Research has indicated that variations in Na + concentration can exert an influence on the process of cellular respiration and energy metabolism [16]. Consequently, it is plausible to suggest that mitochondria, being cellular organelles, may exhibit a heightened sensitivity towards changes in salt concentration. In light of this context, the exposure of astrocytes to a hypertonic saline environment may have noteworthy ramifications on their mitochondrial functionality and, consequently, their state of activation. The primary objective of this investigation was to elucidate the alterations occurring in the mitochondria of astrocytes when exposed to high-salt environments. By doing so, we sought to gain a deeper understanding of the specific impacts of elevated salt consumption on the nervous system.

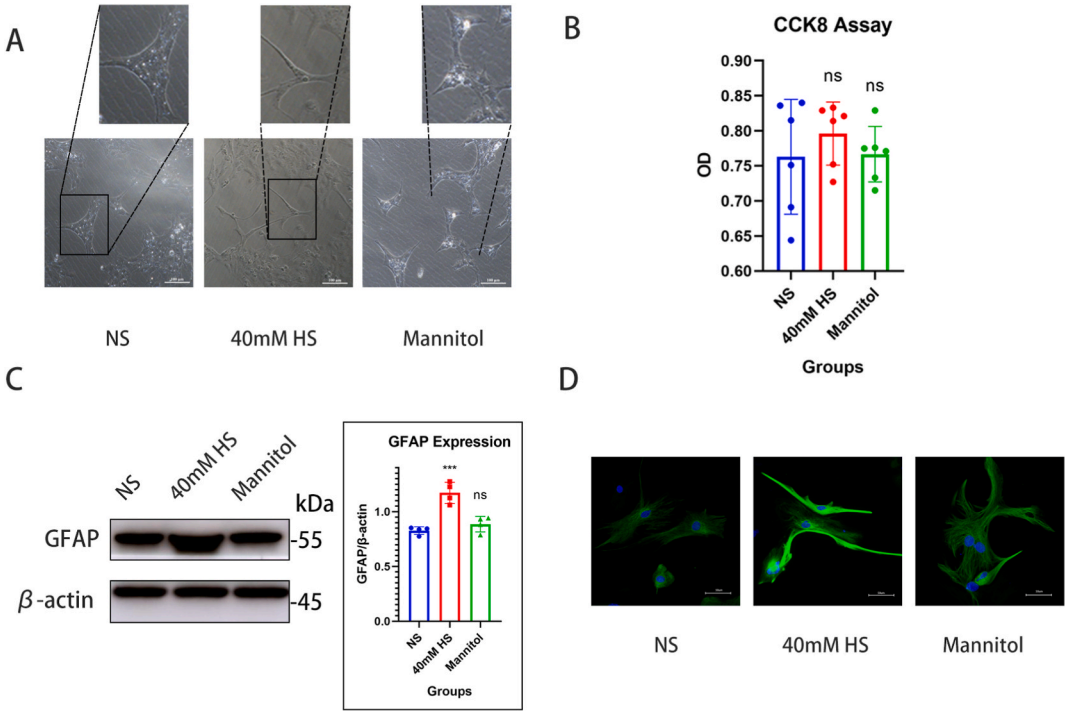

Fig. 1. Changes of astrocyte morphology, cell viability and GFAP in hypersaline state
(A) Right field microscopy images showing astrocyte morphology across treatment groups, normal salt (NS), high salt (40 mM HS), and 80 mM mannitol (Mannitol). (B) Cell Counting Kit 8 (CCK8) assay results to demonstrate astrocyte viability. *P < 0.05, **P < 0.01, compared with NS. (C) Western blot results for glial fibrillary acidic protein (GFAP) expression. *P < 0.05, **P < 0.01, ***P < 0.001 compared with NS. (D) Immunofluorescence images of GFAP (green) and 4′,6-diamidino-2-phenylindole (blue) stained astrocytes.

2. Results

2.1. High salt induces Astrocyte activation without Affecting viability through a mechanism independent of osmotic pressure

According to literature reports and our previous studies, adding an additional 40 mM of sodium chloride is the regimen that best simulates the clinic and has the most obvious effect on astrocytes [8,14,15]. Exposure to additional 40 mM salt concentrations led to astrocyte elongation, as determined by bright-field microscopy (Fig. 1A). The mannitol-treated group, acting as an osmotic control, showed no such alteration; demonstrating that this morphological change was specific to high salt concentrations. Cell viability, as assessed by the Cell Counting Kit 8 (CCK8) assay, was consistent across all groups (Fig. 1B). Furthermore, glial fibrillary acidic protein (GFAP) expression was upregulated in the high salt group, indicating astrocyte activation, whereas it remained unchanged in the mannitol group (Fig. 1C). This result was confirmed by GFAP staining (Fig. 1D).

2.2. High salt induced morphological changes of astrocyte mitochondria and decreased levels of oxidative phosphorylation and glycolysis pathways

Exposure to 40 mM salt resulted in significant transcriptional changes in astrocytes, as evidenced by a total of 1461 upregulated and 1151 downregulated genes when compared to the normal conditions (Fig. 2A). A focused analysis of the downregulated genes using Kyoto Encyclopedia of Genes and Genomes (KEGG) pathway enrichment revealed pronounced suppression of the oxidative phosphorylation and glycolysis pathways (Fig. 2B), highlighting a potential metabolic disruption. Furthermore, high-resolution HIS-SIM images confirmed that the high salt environment induced mitochondrial fragmentation in astrocytes, resulting in a change from their typical interconnected structure (Fig. 2C). These results suggest a potential metabolic distress in these cells when subjected to salt stress.

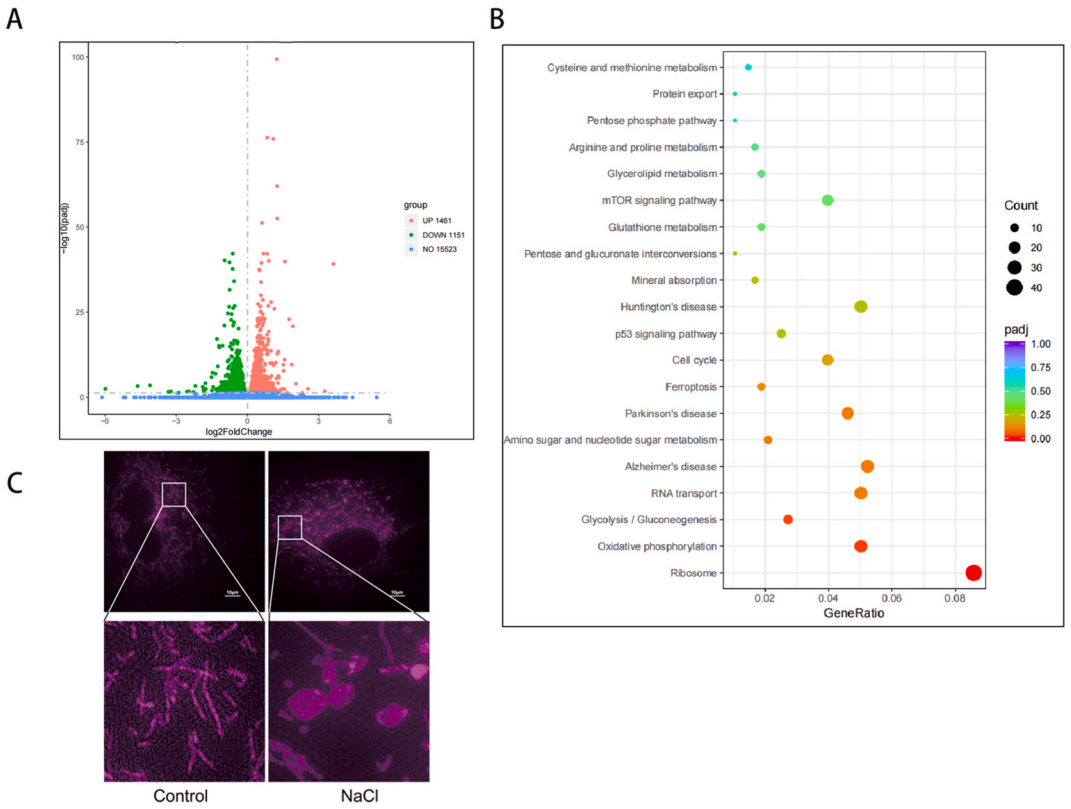

Fig. 2. Transcriptional and Mitochondrial Changes in Astrocytes under High-Salt Conditions.
(A) Volcano plot of the differentially expressed genes in astrocytes exposed to normal (NS) vs. 40 mM high-salt (HS) conditions. (B) Dot plot representation of KEGG pathway enrichment analysis highlighting the downregulation of oxidative phosphorylation and glycolysis pathways under high-salt conditions. (C) HIS-SIM images show the mitochondrial fragmentation in astrocytes under 40 mM high-salt conditions compared to the normal controls.

2.3. Sodium chloride inhibit mitochondrial respiration and suppress the mitochondrial membrane potential in Astrocyte in vitro

Metabolic alterations induced by high salt exposure were investigated using a Seahorse Bioscience extracellular flux analyzer. Real-time measurements revealed significant deviations in the oxygen consumption rate (OCR) across different treatment conditions (Fig. 3A). Specifically, the 40 mM NaCl group showed significant changes, indicating disruption of mitochondrial respiratory function. Additionally, despite the evident variations in OCR, the glycolytic reserve remained largely unaffected across the groups (Fig. 3A).

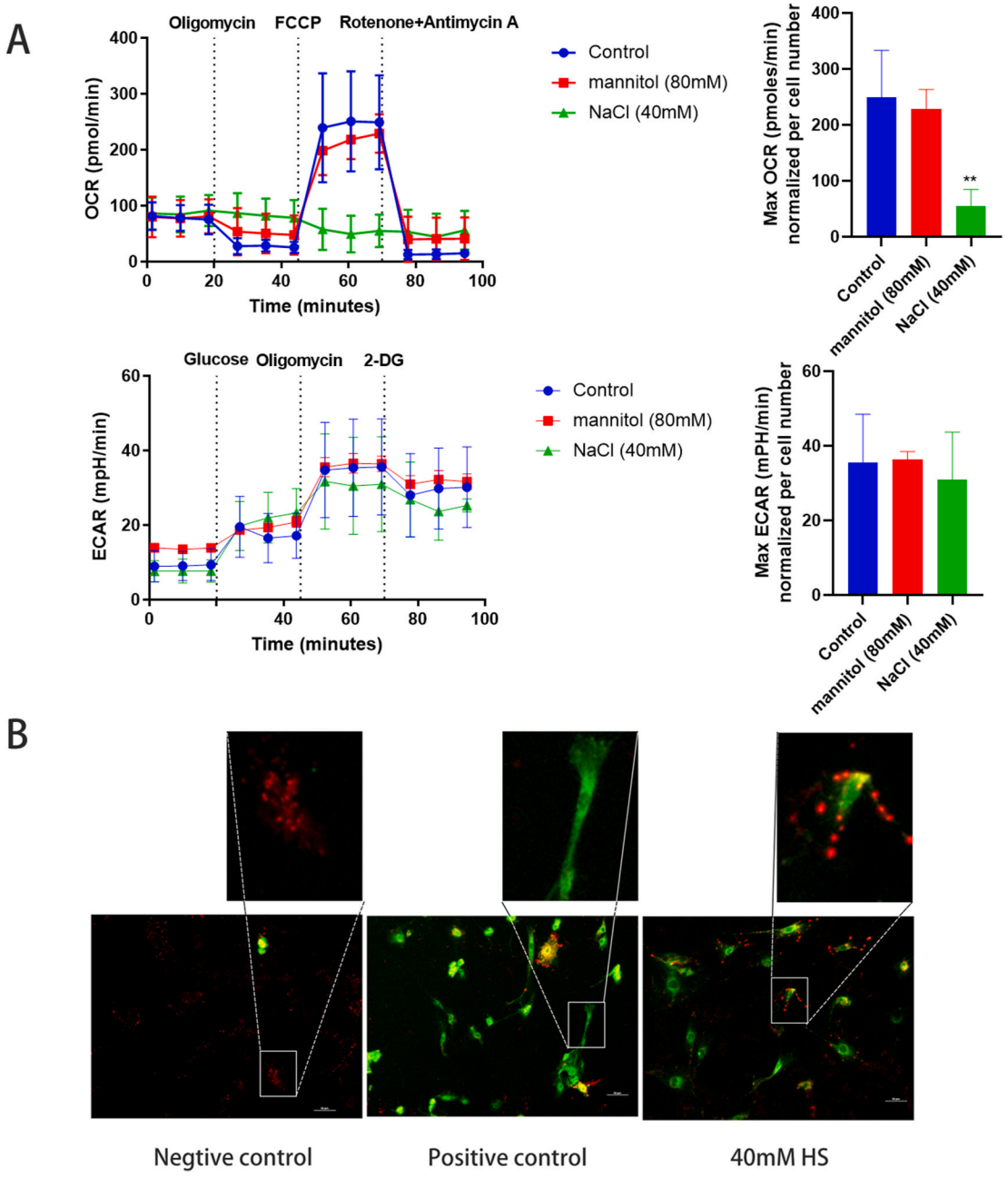

Fig. 3. High salt reduces mitochondrial respiration membrane potential in astrocyte in vitro
(A) Time-dependent effect of high salt (40 mM) treatment and mannitol (80 mM) on the oxygen consumption rate (OCR) and extracellular acidification rate (ECAR). Cells were treated with different medium for the indicated time, and then the OCR of and the ECAR were monitored by using the Seahorse Bioscience extracellular flux analyzer in real time. Dotted lines indicate incubation of cells with the indicated compounds. **$P < 0.01$ compared with control. (B) JC-1 staining to determine mitochondrial membrane potential. JC-1 aggregates in mitochondria with intact membrane potential, leading to red fluorescence. In mitochondria with decreased membrane potential, JC-1 remains in monomeric form in the cytosol, exhibiting green fluorescence.

To gauge mitochondrial health and membrane potential, we performed JC-1 staining. Under high-salt conditions, the sensitive dye JC-1 failed to aggregate within the inner mitochondrial membrane. This led to a shift in fluorescence from the typical red, indicative of healthy mitochondria, to green; indicating a compromised mitochondrial membrane potential in the high-salt group (Fig. 3B). This provides further evidence for the detrimental effects of high salt concentrations on mitochondrial integrity in astrocytes.

2.4. TSPO ligands protect the damaged mitochondria and reduce Abnormal activation of astrocytes in the hypersaline state

We explored the potential of the TSPO drug ligand FGIN-1-27 as a therapeutic strategy to counteract high-salt-induced dysfunction in astrocytes. After FGIN-1-27 treatment, a marked improvement in the mitochondrial network structure was observed, highlighting the pivotal role of FGIN-1-27 in restoring mitochondrial health (Fig. 4A). Furthermore, FGIN-1-27 treatment restored the typical astrocyte morphology (Fig. 4B). Critically, the activation marker GFAP previously upregulated under high-salt conditions returned to baseline levels after treatment with FGIN-1-27 (Fig. 4C and D).

3. Discussion

While salt plays a crucial role in maintaining the water-electrolyte balance, an excessive consumption of salt can lead to various health complications [17]. A diet rich in sodium chloride has been widely recognized for its association with the development of diverse cerebrovascular and systemic vascular conditions, primarily stemming from the presence of elevated blood pressure [18–20]. Recent investigation has revealed that the consumption of a diet rich in salt has the potential to stimulate neurovascular and cognitive impairment. Furthermore, it has been observed that such a diet can worsen the disruption of the blood-brain barrier in cases of permanent cerebral ischemia, regardless of its impact on arterial pressure [21]. Hence, exploring the immediate impacts of a diet rich in sodium on the central nervous system represents a novel avenue of investigation in the field of biology.

Prior research has indicated that an elevated concentration of sodium chloride in the surrounding environment inhibits the functioning of the mitochondrial electron transport chain specifically at Complex II in plasma monocyte phagocytes [16]. In our investigation, the presence of a high concentration of salt in the environment caused disturbances in the functioning of the mitochondria, resulting in a notable reduction in the maximum oxygen consumption rate (OCR) and the occurrence of morphological

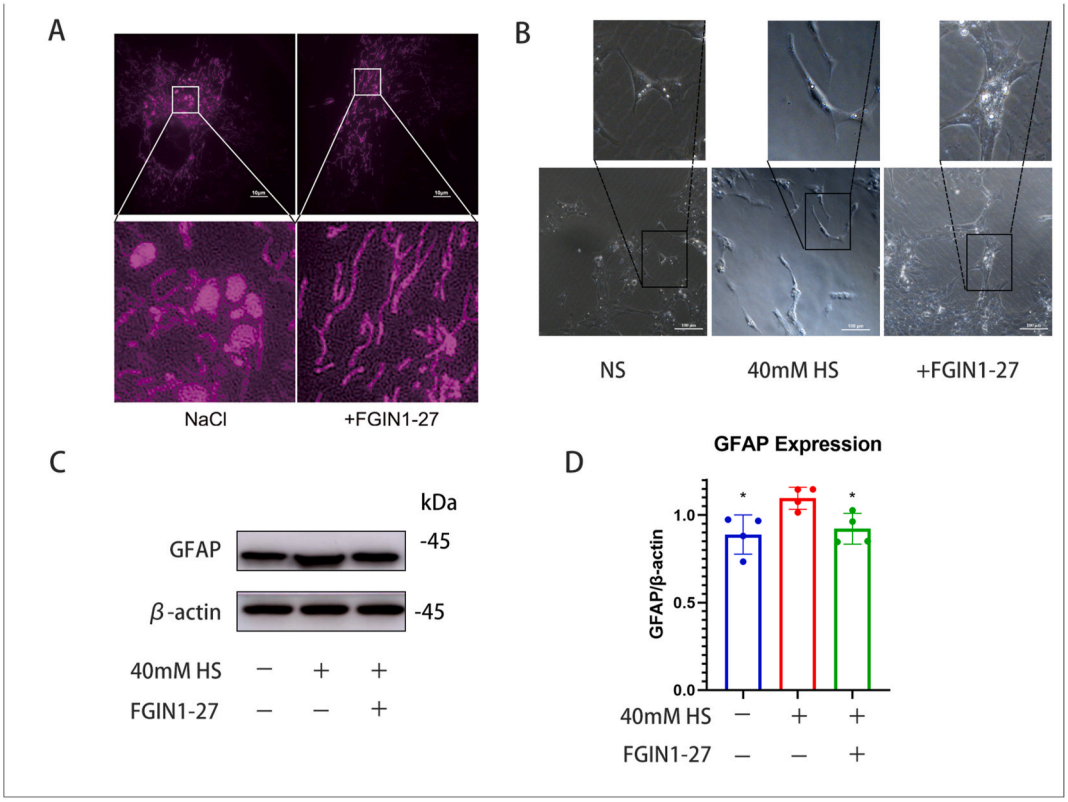

Fig. 4. FGIN-1-27 alleviate the damaged mitochondria and attenuate high salt induced activation of astrocytes
(A) Mitochondrial network structure in astrocytes after FGIN-1-27 treatment. (B) Morphological changes in astrocytes after FGIN-1-27 treatment. (C, D) Western blot analysis of the expression levels of GFAP in astrocytes following FGIN-1-27 treatment. *P < 0.05 compared with 40 mM high-salt conditions (HS). NS, normal salt.

fragmentation. The dysfunction of mitochondrial oxidative phosphorylation can lead to a decline in mitochondrial membrane potential, as indicated by the observed decrease in the red/green fluorescence ratio following JC-1 staining [22].

While astrocytes primarily rely on glycolysis for energy production, they also engage in oxidative phosphorylation (OxPhos) within their mitochondria to metabolize various substrates [23,24]. The brain relies heavily on astrocytic oxidative phosphorylation (OxPhos) for the breakdown of fatty acids and the regulation of lipid balance within the system. When the lipid content becomes too much for the astrocytes' oxidative phosphorylation capacity, increased levels of acetyl-CoA trigger a response in astrocytes by promoting the acetylation and activation of STAT3 [25]. This response is accompanied by an elevation in GFAP expression, alterations in cell shape, and an upregulation of inflammatory molecules [26]. Another plausible scenario entails the activation of STAT3 in tandem with the buildup of acylcarnitines, facilitated by the acetyl-CoA produced through glycolysis. Acylcarnitines, which have been identified as toxic compounds, exhibit increased levels within reactive astrocytes [27,28]. Consequently, the accumulation of these substances may potentially contribute to the progression towards a reactive phenotype.

The 18 kDa translocator protein (TSPO) is a type of protein that spans across the cellular membrane, specifically found predominantly on the outer membrane of mitochondria. It plays a crucial role in facilitating various biological processes, including the production of steroids and the regulation of mitochondrial energy production [29,30]. The TSPO agonist and drug ligand FGIN-1-27 has the ability to maintain the structural integrity of the mitochondrial membrane [31]. In addition, recent studies have shown that FGIN-1-27 can also maintain mitochondrial homeostasis, thereby protecting mitochondrial function [32]. In this investigation, the presence of elevated salt concentrations led to a greater prevalence of fragmented mitochondria as opposed to tubular mitochondria. Nevertheless, the administration of FGIN-1-27 exhibited a notable amelioration in the structural characteristics of the mitochondria, while concurrently reversing the heightened activation state of astrocytes in the presence of elevated salt concentrations. This suggests that the astrocyte's physiological condition may be influenced by the impact of a high salt environment on mitochondrial functionality.

Although our study provides valuable insights into the interactions between astrocytes and the elevated sodium levels, there are some limitations that need to be addressed. The most notably is the absence of corroboration from in vivo experiments, which constitutes a pivotal aspect of our forthcoming research. Additionally, this is only an observational study of astrocyte activation and mitochondrial hyperfunction under high salt condition, both of which can be alleviated with FGIN-1-27. However, the causal relationship between these two phenomena remains to be well explained. Future studies should focus on elucidating the detailed molecular mechanisms which may involve the use of gene knockout or knockdown techniques to determine the specific targets of FGIN-1-27. Finally, adding additional sodium chloride also increases chloride concentration, but we did not take into account the effect of elevated chloride on astrocytes. Few studies have looked at the direct effects of changes in chloride ions on CNS cells. Previous research has found that alterations in chloride concentration can influence excitability of neurons [33]. In addition, the alteration of chloride channels has an important effect on the structure and roles in brain homeostasis of astrocytes [34]. The effect of elevated chloride on astrocytes needs to be further investigated.

In brief, this investigation unveils that elevated levels of sodium can directly stimulate astrocytes and hinder the functionality of mitochondria, offering fresh evidence regarding the detrimental impacts of excessive sodium intake on the nervous system. These discoveries illuminate the potential biological processes that may be responsible for the development of neurological disorders induced by high salt intake. Additional explorations into the modulation of astrocytic mitochondrial homeostasis have the potential to unveil novel therapeutic avenues in combating the neurotoxic effects induced by excessive salt levels. The findings of our study underscore the significance of regulating dietary sodium consumption in order to uphold the integrity of the nervous system.

4. Methods

4.1. Isolation of astrocytes and culture

Primary astrocytes from the cerebral cortex, which is the part of the interstitial rich in microvessels and is more susceptible to high-salt environment, were isolated from 1-day-old C57 mouse as described previously [14,35]. Cells were cultured alone on plates. All experiments were conducted using 80%–85 % confluent cells. Before each experiment, the plated cells were incubated with serum-free Dulbecco's Modified Eagle Medium (DMEM) medium for 1 h. After this, the medium was replaced with serum-free DMEM containing NaCl (Sigma-Aldrich, St. Louis, MO, USA) at concentrations of 0/40 mM (0 mM received equivalent volumes of the dimethyl sulfoxide (DMSO)) or 80 mM mannitol (Sigma-Aldrich) for 24 h. Prior to use, FGIN-1-27 N, N-Dihexyl-2-(4-fluorophenyl) indole-3-acetamide 2-(4-fluorophenyl)-N (FGIN-1-27; Sigma-Aldrich; D8555) was dissolved in DMSO, and stored as a stock solution of 0.1M at −20 °C. The treatment with FGIN-1-27 was performed by adjusting the final concentration to 0.04 % with DMSO in the culture media.

4.2. Cell viability assay

Primary astrocytes were detached using 0.25 % trypsin-EDTA for 3 min at 37 °C in a CO_2 incubator. The trypsinization was halted by adding an equal volume of serum-containing DMEM, followed by centrifugation at 1200*g* for 5 min at room temperature. The supernatant was discarded, and the cells were resuspended in serum-free DMEM for subsequent assays. Cell viability was measured using a Cell Counting Kit 8 (CCK8; Sigma-Aldrich), according to the manufacturer's protocol. Briefly, the cells in each treatment group were transferred to 96-well plates at a density of 5×10^3 cells per well in a volume of 100 μL. Ten microliters of CCK8 assay solution was added to each well and incubated for 4 h at 37 °C. Cell number and viability were calculated by measuring the absorbance at a wavelength of 450 nm using a multiplate reader (BIO-TEK, Winooski, VT, USA).

4.3. Western blot analysis

Astrocytes were collected and homogenized in radioimmunoprecipitation assay buffer containing a protease inhibitor cocktail (Sigma-Aldrich), followed by a 15 min incubation on ice. The supernatant was obtained by centrifuging at 12,000×*g* for 20 min at 4 °C. The total protein concentration in each sample was quantified using the BCA assay (Thermo Fisher Scientific, Waltham, MA, USA), according to the manufacturer's instructions. Equal amounts of protein were separated by sodium dodecyl sulfate-polyacrylamide gel electrophoresis and transferred to Immobilon-P membranes (Millipore, Burlington, MA, USA) for 1 h. The membranes were then blocked for 1 h using 5 % non-fat dry milk dissolved in TBST (Tris-buffered saline with 0.1 % Tween 20) and incubated with mouse monoclonal anti-glial fibrillary acidic protein antibody (anti-GFAP; 1:1000, Cell Signaling Technology, Danvers, MA, USA; #3670) at 4 °C overnight. After washing three times, the membranes were treated with the appropriate secondary antibody (1:2000) at room temperature for 1 h. To verify that equal amounts of protein were loaded, blots were also probed with antibodies against β-Actin (1:2000, Cell Signaling Technology, #3700). Target proteins were visualized using the ECL kit (Millipore). ImageJ software was used to determine the relative density of signal expression.

4.4. Immunofluorescence staining

Astrocytes were plated on poly L-lysine-treated coverslips. Following each treatment, cells were fixed in 4 % paraformaldehyde for 20 min and blocked with 10 % goat serum in phosphate-buffered saline (PBS). Slides were incubated overnight in a humidified chamber at 4 °C with the primary antibodies, mouse monoclonal anti-GFAP (1:400; Cell Signaling Technology; #3670). After primary antibody incubation, the samples were washed and incubated in the appropriate fluorescent-conjugated secondary antibody, Goat Anti-Mouse IgG (H + L) FITC-conjugated (1:400; Affinity Biosciences, Cinncinnati, OH, USA; #S0007), for 1 h. The cells were counterstained with 4′,6-diamidino-2-phenylindole. The images were captured using an IX71 fluorescence microscope (Olympus, Tokyo, Japan).

4.5. RNA extraction and sequencing library preparation

Total RNA was extracted using the TRIzol reagent (Thermo Fisher Scientific), according to the manufacturer's instructions. The RNA concentration and purity were measured using a NanoDrop™ 2000 (Thermo Fisher Scientific), with the purity of RNA assessed using the A260/A280 ratio, where a threshold of 1.8–2.0 was set for acceptable purity. RNA integrity by an RNA Nano 6000 Assay Kit using the Agilent Bioanalyzer 2100 system (Agilent Technologies, Santa Clara, CA, USA). A 1 μg RNA input was used to prepare sequencing libraries using the Hieff NGS Ultima Dual-mode mRNA Library Prep Kit for Illumina (Yeasen Biotechnology Co., Ltd., Shanghai, China), according to the manufacturer's instructions, and index codes were added to assign sequences to each sample. The libraries were sequenced on an Illumina NovaSeq (San Diego, CA, USA) to generate 150 bp paired-end reads, according to the manufacturer's instructions.

4.6. Data analysis

Raw data in fastq format were first processed using in-house Perl scripts to obtain clean data by removing the reads containing adapters, poly-N, and those of low-quality. The Q20, Q30, GC content, and sequence duplication levels of the clean data were also calculated. All the downstream analyses were based on high-quality clean data. The HISAT2 tool was used to map reference genomes, and only reads with a perfect match or one mismatch were further analyzed and annotated based on the reference genome. The StringTie Reference Annotation Based Transcript (RABT) assembly method was used to construct and identify both known and novel transcripts from the HISAT2 alignment results. Gene functions were annotated based on the following databases: Nr (NCBI non-redundant protein sequences), Pfam (protein family), KOG/COG (Clusters of Orthologous Groups of proteins), Swiss-Prot (a manually annotated and reviewed protein sequence database), KO (KEGG Ortholog database), and GO (Gene Ontology). Gene expression levels were quantified as fragments per kilobase of transcript per million mapped fragments.

4.7. Differential expression analysis and KEGG pathway enrichment analysis

Differential expression analysis of the two groups was performed using the DESeq2. The resulting P values were adjusted using the Benjamini and Hochberg method to control for the false discovery rate. Genes with an adjusted P-value$<$0.01 & Fold Change$\geq$2 were considered differentially expressed. We used KOBAS [36] and Cluster Profiler software to analyze the statistical enrichment of expression genes in the KEGG pathways.

4.8. High Intelligent and sensitive SIM (HIS-SIM) imaging

Super-resolution imaging of mitochondrial structures was performed using commercialized HIS-SIM provided by Guangzhou Computational Super-resolution Biotech Co., Ltd. Images were acquired using a 100 × (N.A. 1.5) oil immersion objective (Olympus). The cells were seeded in 8-well chambered coverglass and stained with 500 nM MitoTracker Red CMXRos (Cell Signaling Technology; 9082S) and 0.5 % dimethyl sulfoxide in DMEM + for 2 h in a CO2 incubator. The cells were then washed three times with fresh medium to remove unbound dye and maintained in DMEM + at 37 °C and 5 % CO2 in a humidified chamber for live SIM imaging. SIM images

were collected and analyzed as previously described [37]. Sparse deconvolution was performed to further improve the image quality [38].

4.9. Seahorse extracellular flux assay

The OCR and ECAR were determined using the Seahorse XF Cell Mito Stress Test Kit (Agilent Technologies; 103015-100) and Seahorse XF Glycolysis Stress Test Kit (Agilent Technologies; 103020-100), according to the manufacturer's instructions. Briefly, 3×10^5 primary astrocyte per well were seeded onto Seahorse XF 96-well culture microplates and cultured overnight. Before measurement, the cells were washed twice and then maintained with the XF assay medium (Agilent Technologies; 102353-100). After baseline measurements; oligomycin, carbonyl cyanide p-trifluoromethoxyphenylhydrazone, rotenone, and antimycin A were sequentially injected into the wells at specific time points for OCR analysis. For the ECAR analysis; glucose, oligomycin, and 2-DG were injected. Seahorse XF 96 Wave software was used to analyze the data. The results were normalized to the cell number and the data are presented as pmol/min for OCR and mPH/min for ECR.

4.10. Mitochondrial membrane potential assessment

The JC-1 probe was used to measure mitochondrial depolarization in astrocytes, according to the manufacturer's instructions. Briefly, the astrocytes were cultured in 24-well plates. At the end of treatment, culture medium was removed and the cells were incubated with JC-1 staining solution at a final concentration of 5 μg/mL for 20 min at 37 °C. The cells were then rinsed twice with PBS and excited at 488 nm using a fluorescence microscope (Nikon E600, Tokyo, Japan). The JC-1 dye undergoes a reversible change in fluorescence emission from green to greenish orange as ΔΨ increases. Cells with high ΔΨ form JC-1 aggregates and fluoresce red; those with low ΔΨ contain monomeric JC-1 and fluoresce green.

4.11. Statistical analysis

All data are presented as the mean ± SEM. Statistical analyses were performed using GraphPad Prism version 8.0 (GraphPad Software, Boston, MA, USA). The significance of the differences was calculated using Student's t-test or by one-way or two-way analysis of variance (ANOVA), followed by Tukey's multiple comparison test. For all tests, statistical significance was set at $P < 0.05$.

CRediT authorship contribution statement

Yuemin Qiu: Writing – original draft, Project administration, Methodology, Formal analysis, Data curation. **Gengxin Lu:** Project administration, Methodology, Data curation. **Shifeng Zhang:** Methodology, Formal analysis. **Li Minping:** Project administration, Methodology. **Xu Xue:** Project administration, Methodology. **Wu Junyu:** Project administration, Formal analysis. **Zhihui Zheng:** Project administration, Formal analysis. **Weiwei Qi:** Project administration, Funding acquisition. **Junjie Guo:** Project administration, Formal analysis. **Dongxiao Zhou:** Software, Project administration. **Haiwei Huang:** Visualization, Validation, Supervision, Funding acquisition. **Zhezhi Deng:** Writing – review & editing, Visualization, Validation, Methodology, Funding acquisition, Conceptualization.

Data availability statement

Data will be made available on request. The data that support the findings of this study are available from the corresponding author, DZZ&HHW, upon reasonable request.

Funding

This study was supported by grants from Guangzhou Science and Technology Program key projects (202206010097), Guangzhou Science and Technology Program projects (2023A04J2199), Guangdong Basic and Applied Basic Research Foundation (2020A1515110153, 2023A1515010491), National Natural Science Foundation of China (81971166, 82271410), Guangzhou Basic and Applied Basic Research Foundation (2024A04J4565), the Southern China International Cooperation Base for Early Intervention and Functional Rehabilitation of Neurological Diseases (2015B050501003), Guangdong Provincial Engineering Center For Major Neurological Disease Treatment, Guangdong Provincial Translational Medicine Innovation Platform for Diagnosis and Treatment of Major Neurological Disease, Guangdong Provincial Clinical Research Center for Neurological Diseases. including the design of the study, experiment, analysis, and interpretation of data and in writing the manuscript.

Declaration of competing interest

The authors declare that they have no known competing financial interests or personal relationships that could have appeared to influence the work reported in this paper.

Acknowledgement

We thank Guangzhou CSR Biotech Co. Ltd for live-cell imaging by using their commercial super-resolution microscope (HIS-SIM), data acquisition, SR image reconstruction, analysis and discussion.

Abbreviation:

CCK8	cell counting kit 8
CNS	central nervous system
ECAR	extracellular acidification rate
GFAP	glial fibrillary acidic protein
HIS-SIM	High Intelligent and Sensitive SIM
KEGG	Kyoto Encyclopedia of Genes and Genomes
OCR	oxygen consumption rate
OxPhos	oxidative phosphorylation
TSPO	translocator protein

References

[1] T.A. Kotchen, A.W. Cowley, Frohlich ED. Jr, Salt in health and disease—a delicate balance, New Eng J Med 368 (2013) 1229–1237.
[2] D.B. Hipgrave, S. Chang, X. Li, Y. Wu, Salt and sodium intake in China, JAMA 315 (7) (2016).
[3] B. Michael, P. Zemel, J.R. Sowers, M.D. Salt, Sensitivity and systemic hypertension in the Elder, Am J Cardidol 61 (1988) 7H–12H.
[4] A. Machnik, W. Neuhofer, J. Jantsch, A. Dahlmann, T. Tammela, K. Machura, et al., Macrophages regulate salt-dependent volume and blood pressure by a vascular endothelial growth factor-C-dependent buffering mechanism, Nat Med 15 (2009) 545–552.
[5] A. Mente, M. O'Donnell, S. Rangarajan, G. Dagenais, S. Lear, M. McQueen, et al., Associations of urinary sodium excretion with cardiovascular events in individuals with and without hypertension: a pooled analysis of data from four studies, Lancet 388 (10043) (2016) 465–475.
[6] A. Mente, M. O'Donnell, S. Rangarajan, M. McQueen, G. Dagenais, A. Wielgosz, et al., Urinary sodium excretion, blood pressure, cardiovascular disease, and mortality: a community-level prospective epidemiological cohort study, Lancet 392 (2018) 496–506.
[7] K. Stolarz-Skrzypek, T. Kuznetsova, L. Thijs, V. Tikhonoff, J. Seidlerova, T. Richart, et al., Fatal and nonfatal outcomes, incidence of hypertension, and blood pressure changes in relation to urinary sodium excretion, JAMA 305 (2011) 1777–1785.
[8] K.J. Binger, M. Gebhardt, M. Heinig, C. Rintisch, A. Schroeder, W. Neuhofer, D.N. Müller, High salt reduces the activation of IL-4- and IL-13-stimulated macrophages, J Clin Investigat 125 (11) (2015) 4223–4238.
[9] M.V. Sofroniew, H.V. Vinters, Astrocytes: biology and pathology, Acta Neuropathol. 119 (2010) 7–35.
[10] L. Ben Haim, D.H. Rowitch, Functional diversity of astrocytes in neural circuit regulation, Nat. Rev. Neurosci. 18 (1) (2017) 31–41.
[11] M.M. Halassa, P.G. Haydon, Integrated brain circuits: astrocytic networks modulate neuronal activity and behavior, Ann Rev Physiol 72 (2010) 335–355.
[12] B.S. Khakh, M.V. Sofroniew, Diversity of astrocyte functions and phenotypes in neural circuits, Nat. Neurosci. 18 (2015) 942–952.
[13] F. Vasile, E. Dossi, N. Rouach, Human astrocytes: structure and functions in the healthy brain, Brain Struct. Funct. 222 (5) (2017) 2017–2029.
[14] Z. Deng, Y. Wang, L. Zhou, Y. Shan, S. Tan, W. Cai, et al., High salt-induced activation and expression of inflammatory cytokines in cultured astrocytes, Cell Cycle 16 (2017) 785–794.
[15] Z. Deng, L. Zhou, Y. Wang, S. Liao, Y. Huang, Y. Shan, et al., Astrocyte-derived VEGF increases cerebral microvascular permeability under high salt conditions, AGING-US 12 (12) (2020) 11781–11793.
[16] S. Geisberger, H. Bartolomaeus, P. Neubert, R. Willebrand, C. Zasada, T. Bartolomaeus, et al., Salt transiently inhibits mitochondrial energetics in mononuclear phagocytes, Circulation 144 (2021) 144–158.
[17] I.J. Brown, I. Tzoulaki, V. Candeias, P. Elliott, Salt intakes around the world: implications for public health, Intl J Epidemiol 38 (3) (2009) 791–813.
[18] D. Mozaffarian, S. Fahimi, G.M. Singh, R. Micha, S. Khatibzadeh, R.E. Engell, et al., Global sodium consumption and death from cardiovascular causes, New Eng J Med 371 (2014) 624–634.
[19] P.R. Conlin, Eat your fruits and vegetables but hold the salt, Circulation 116 (2007) 1530–1531.
[20] M. O'Donnell, A. Mente, S. Yusuf, Sodium intake and cardiovascular health, Circulat Res 116 (2015) 1046–1057.
[21] M. Sumiyoshi, K.T. Kitazato, K. Yagi, T. Miyamoto, Y. Kurashiki, N. Matsushita, et al., The accumulation of brain water-free sodium is associated with ischemic damage independent of the blood pressure in female rats, Brain Res. 1616 (2015) 37–44.
[22] F. Sivandzade, A. Bhalerao, L. Cucullo, Analysis of the mitochondrial membrane potential using the cationic JC-1 dye as a sensitive fluorescent probe, Bio-Protocol 9 (1) (2019).
[23] A. Almeida, J. Almeida, J.P. Bolaños, S. Moncada, Different responses of astrocytes and neurons tonitric oxide: the role of glycolytically generated ATP in astrocyte protection, Proc. Natl. Acad. Sci. USA 98 (2001) 15294–15299.
[24] Y. Mi, G. Qi, F. Vitali, Y. Shang, A.C. Raikes, T. Wang, et al., Loss of fatty acid degradation by astrocytic mitochondria triggers neuroinflammation and neurodegeneration, Nat Metabol 5 (2023) 445–465.
[25] L.F. Rubio-Atonal, M.S. Ioannou, Astrocytic OxPhos: more than just energy production, Nat Metabol 5 (2023) 362–363.
[26] S.A. Liddelow, B.A. Barres, Reactive astrocytes: production, function, and therapeutic potential, Immunity 46 (2017) 957–967.
[27] T. Nguyen, Bea. DGAT1-dependent lipid droplet biogenesis protects mitochondrial function during starvation-induced autophagy, Develop Cell 42 (2017) 9–21.
[28] K.A. Guttenplan, M.K. Weigel, P. Prakash, P.R. Wijewardhane, P. Hasel, U. Rufen-Blanchette, et al., Neurotoxic reactive astrocytes induce cell death via saturated lipids, Nature 599 (2021) 102–107.
[29] J. Gatliff, D. East, J. Crosby, R. Abeti, R. Harvey, W. Craigen, et al., TSPO interacts with VDAC1 and triggers a ROS-mediated inhibition of mitochondrial quality control, Autophagy 10 (2014) 2279–2296.
[30] S. Bader, L. Wolf, V.M. Milenkovic, M. Gruber, C. Nothdurfter, R. Rupprecht, C.H. Wetzel, Differential effects of TSPO ligands on mitochondrial function in mouse microglia cells, Psychoneuroendocrinology 106 (2019) 65–76.
[31] R.R. Anholt, P.L. Pedersen, E.B. De Souza, S.H. Snyder, The peripheral-type benzodiazepine receptor. Localization to the mitochondrial outer membrane, J. Biol. Chem. 261 (2) (1986) 576–583.
[32] Y. Zhang, J. He, Z. Yang, H. Zheng, H. Deng, Z. Luo, et al., Preventative effect of TSPO ligands on mixed antibody-mediated rejection through a Mitochondria-mediated metabolic disorder, J. Transl. Med. 21 (1) (2023) 295.
[33] P. Blaesse, M.S. Airaksinen, C. Rivera, K. Kaila, Cation-chloride cotransporters and neuronal function, Neuron 61 (2009) 820–838.

[34] X. Elorza-Vidal, H. Gaitan-Penas, R. Estevez, Chloride channels in astrocytes: structure, roles in brain homeostasis and implications in disease, Int. J. Mol. Sci. 20 (5) (2019).
[35] L.L. Rubin, D.E. Hall, S. Porter, K. Barbu, C. Cannon, H.C. Horner, et al., A cell culture model of the blood-brain barrier, J. Cell Biol. 115 (1991) 1725–1735.
[36] X. Mao, T. Cai, J.G. Olyarchuk, L. Wei, Automated genome annotation and pathway identification using the KEGG Orthology (KO) as a controlled vocabulary, Bioinformatics 21 (19) (2005) 3787–3793.
[37] X. Huang, J. Fan, L. Li, H. Liu, R. Wu, Y. Wu, et al., Fast, long-term, super-resolution imaging with Hessian structured illumination microscopy, Nat. Biotechnol. 36 (2018) 451–459.
[38] W. Zhao, S. Zhao, L. Li, X. Huang, S. Xing, Y. Zhang, et al., Sparse deconvolution improves the resolution of live-cell super-resolution fluorescence microscopy, Nat. Biotechnol. 40 (4) (2022) 606–617.